The Astrophysical Journal, 903:10 (8pp), 2020 November 1 https://doi.org/10.3847/1538-4357/abb5f4
© 2020. The American Astronomical Society. All rights reserved.

NGC 6822 as a Probe of Dwarf Galactic Evolution*

Brent Belland[1], Evan Kirby[1], Michael Boylan-Kolchin[2], and Coral Wheeler[3,4]
[1] California Institute of Technology, 1200 East California Boulevard, Pasadena, CA 91125, USA; bbelland@caltech.edu
[2] The University of Texas at Austin, 2515 Speedway, Stop C1400, Austin, TX 78712, USA
[3] Carnegie Observatories, 813 Santa Barbara Street, Pasadena, CA 91101, USA
Received 2020 July 8; revised 2020 September 4; accepted 2020 September 5; published 2020 October 26

Abstract

NGC 6822 is the closest isolated dwarf irregular galaxy to the Milky Way. Its proximity and stellar mass ($10^8 M_\odot$, large for a dwarf galaxy) allow for a detailed study of its kinematic properties. The red giant branch (RGB) stars at the galaxy's center are particularly interesting because they are aligned on an axis perpendicular to the galaxy's more extended H I disk. We detected a velocity gradient among the RGB population using spectra from Keck/Deep Imaging Multi-Object Spectrograph (DEIMOS). This rotation is aligned with the H I disk, but the sense of rotation is about the major axis of the central RGB population. We measured the rotation velocity (v) and velocity dispersion (σ) of the RGB population in five metallicity bins. We found an increase of rotation support (v/σ) with increasing metallicity, driven primarily by decreasing dispersion. We also deduced an increasing radial distance for lower metallicity stars at -0.5 kpc dex^{-1} by relating the observed stellar kinematics to position via NGC 6822's H I velocity curve. While the inverted metallicity gradient-like distribution could be interpreted as evidence for an outside-in formation scenario, it may instead indicate that stellar feedback disturbed a centrally star-forming galaxy over time.

Unified Astronomy Thesaurus concepts: Dwarf irregular galaxies (417); Stellar kinematics (1608)

1. Introduction

There is a broad set of morphologies that describe massive galaxies (Sandage 2005). Perhaps the best-known morphology difference is between spiral and elliptical galaxies, as in Hubble's classification system Hubble (1926). This visual distinction informs us about some of the physical properties of these galaxies: spiral galaxies contain neutral and ionized gas, actively form stars, and rotate, whereas elliptical galaxies are old, gas poor, quiescent, and supported by random motion (i.e., dispersion).

Galaxies obey a morphology–density relation (Postman & Geller 1984). In denser environments, the population fraction of spiral galaxies decreases, and the fraction of elliptical galaxies increases. This relation points to the formation mechanism of elliptical galaxies: in denser galactic environments, the spiral galaxies begin to merge. These mergers cause gas loss, star formation, and disruption of the rotation support. The result is the transformation of a spiral galaxy into an elliptical galaxy.

For dwarf galaxies, there is a parallel between the spirals and ellipticals. Dwarf irregulars are analogous to giant spirals because they are gas rich, rotating, and star forming. Dwarf spheroidals are analogous to giant ellipticals because they are gas poor, dispersion supported, and quenched. Dwarf galaxies also obey their own morphology–density relation. A dwarf galaxy's morphology is correlated with the distance to its host galaxy. As found by Spekkens et al. (2014), dwarf galaxies within the Milky Way (MW) viral radius are predominantly gas poor (i.e., dwarf spheroidal, dSph), while those just outside the MW viral radius are primarily gas rich (i.e., dwarf irregulars, dIrr).

Mayer et al. (2001) proposed a mechanism, called tidal stirring, to describe this morphology–density relation. Successive pericentric passages near the MW can tidally disturb a dIrr. The ram pressure stripping and tidal influence of the MW cause angular momentum of the galaxy's gas to flow outward. Then, the angular momentum is carried away when the outlying stars and gas are stripped from the galaxy. The loss of rotation and gas thus transitions the dIrr to a dSph and can explain the morphology–density relation.

However, in practice, the "rotation support" (ratio of rotation velocity divided by velocity dispersion) of the old populations in dIrrs is almost uniformly low and consistent with no rotation. This quality holds for both observed galaxies and galaxies simulated by the Feedback in Realistic Environments (Hopkins et al. 2014) code (Wheeler et al. 2017). This is not a surprise for the dSphs, which are dispersion dominated, but dIrrs are usually presumed to form with rotation. Kaufmann et al. (2007) note that, due to their lower mass, dwarf galaxies are more affected by pressure support from gas temperature, which causes them to be less disky and less rotation supported than their more massive counterparts. Nonetheless, some dIrrs clearly have rotating gas disks (e.g., Iorio et al. 2017). What removes the rotation support from a dwarf irregular if not tidal stirring?

One of the most accessible dwarf irregular galaxies to study is NGC 6822. NGC 6822 is about 500 kpc from the MW, making it the nearest isolated dIrr. It is relatively massive, with $10^8 M_\odot$ in stars and a similar mass of H I gas (McConnachie 2012). Its large angular extent (about $1.^\circ 2$) permits studies at high angular resolution. Spectroscopic studies enjoy the luxury of choosing individual stars and achieving a high signal-to-noise ratio for each star observed.

NGC 6822 has many interesting properties that contain clues about its history. NGC 6822 has an optically bright center,

* The data presented herein were obtained at the W. M. Keck Observatory, which is operated as a scientific partnership among the California Institute of Technology, the University of California and the National Aeronautics and Space Administration. The Observatory was made possible by the generous financial support of the W. M. Keck Foundation.
[4] NASA Hubble Fellow.

often referred to as a bar due to its elongated shape (Gallart et al. 1996). As a result, NGC 6822 is classified as an irregular barred dwarf galaxy (de Vaucouleurs et al. 1976). Although the classification of the bar is based simply on the galaxy's visual appearance, Valenzuela et al. (2007) raised the possibility that the central stellar population is a dynamical bar. However, there is also an H I disk that runs normal to this bright optical center de Blok & Walter (2000). Ongoing star formation closely follows the shape of the disk (Komiyama et al. 2003). There also is an older/intermediate-age stellar population associated with NGC 6822 that extends much farther than the bright optical center and does not follow the disk (Letarte et al. 2002; Thompson et al. 2016).

On top of the stellar population distributions, the H I gas disk has unique properties that are worthy of mention. There is a large H I hole and in the southeast of the galaxy and a H I overdensity in the northwest of the galaxy (de Blok & Walter 2000). de Blok & Walter (2000) noted that the southwest of NGC 6822 had a tidal arm feature, indicating a previous interaction history. They estimated that the H I hole had a relatively short kinematic age of 100 Myr, which could be correlated to the tidal arm feature if such an interaction increased the star formation rate. Noting the asymmetrically large mass distribution in the northwest of NGC 6822, they calculated a similar interaction timescale of 300 Myr if the overdensity in the northwest were a merger that had disrupted the southeastern hole, leading to a prediction that the northwest cloud was a companion galaxy. de Blok & Walter (2006) expanded on this interpretation, finding that the cloud was distinguishable from the rest of NGC 6822 in velocity and would have a dynamical mass ratio consistent with a dwarf galaxy merger. However, Cannon et al. (2012) later found that the putative companion had a similar star formation history as the rest of NGC 6822 and no old star overdensity or metallicity difference relative to the expected value from NGC 6822 at its distance. The stellar population was thus inconsistent with dwarf galaxy merger, even though they did not rule out a H I cloud.

This paper addresses the formation history of NGC 6822 by analysis of the kinematics of the old, central population of stars. Section 2 presents the already-published spectra and velocity measurements. Section 3 gives our measurements of rotation and velocity dispersion in different bins of stellar metallicity. We interpret these trends in Section 4, and we summarize in Section 5.

2. Data

Kinematic data for NGC 6822 stars comes from the observations of Kirby et al. (2013). Two-hundred-and-ninety-nine stars between two slitmasks were observed in the Keck II telescope's Deep Imaging Multi-Object Spectrograph (DEIMOS; Faber et al. 2003) with total exposure times of 8.7 and 6.0 hr. The color–magnitude diagram of stars in the Kirby et al. (2013) data is recreated in Figure 1.

Previous analysis of NGC 6822 by Kirby et al. (2014) indicated that rotation might be present in NGC 6822 on the order of 10 km s^{-1}, but a definitive detection of rotation was uncertain due to the high-velocity dispersion of 23.2 ± 1.2 km s^{-1}. Thompson et al. (2016) later found rotation in carbon stars in a more extended population at 11.2 ± 2.1 km s^{-1} with a position angle of 26° ± 13°. A similar rotation was also found in the gas (for example, see Weldrake et al. 2003).

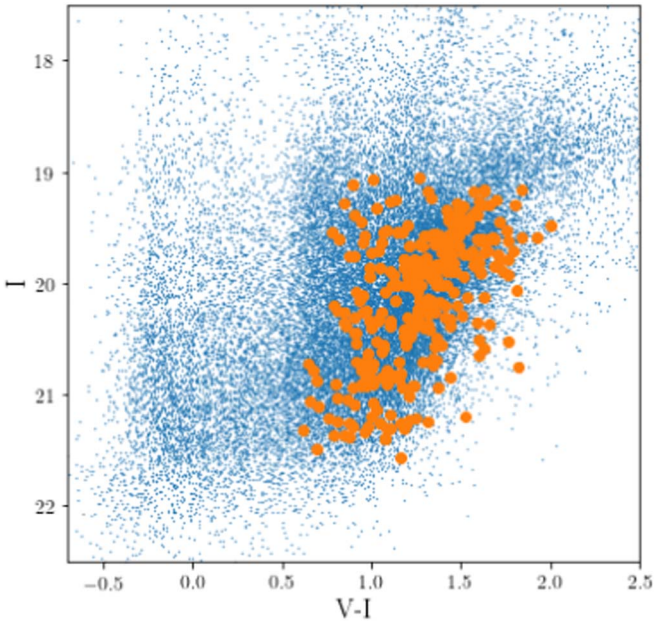

Figure 1. Distribution of stars (orange) from Kirby et al. (2013) in color–magnitude space plotted with photometry (blue) from Massey et al. (2007).

The red giant branch star selection was done by selecting stars within a brightness, color, and isochrone cutoff. Target selection was completed using photometry data from Massey et al. (2007). In this paper, the ages of stars are inferred from the metallicity of the stars, which itself is highly correlated with color. Therefore, any color cutoffs used in the star selection will impact the age/metallicity range considered. Stars with extinction-corrected magnitudes between 19.0 and 21.6 were selected based on the expected brightness of red giants at a distance modulus of 23.40 (479 kpc) (Feast et al. 2012). We applied a constant reddening correction of $E(B-V) = 0.25$ (Massey et al. 2007). Stars beyond the colors between $0.6 < (V-I)_0 < 2.5$ were excluded based on the expected colors of red giants. Yonsei-Yale isochrones in V and I filters ranging from the bluest (2 Gyr, [Fe/H] = −3.76) to the reddest (14 Gyr, metal-rich [Fe/H] = +0.05) bounded the selection in the color–magnitude diagram. In cases where multiple stars competed for the same slit, priority was placed on stars closest to a 6 Gyr, [Fe/H] = −1.05 isochrone.

Especially as this study relies on observing stars with a span of metallicity/ages, it is important to determine possible observation bias. The selection of red giant branch stars in Kirby et al. (2013) was designed to be as inclusive as possible: the large isochrone metallicity range of −3.76 to +0.05 and large isochrone age range of 2–14 Gyr is expected to not reject any red giant branch star, thus not biasing the metallicity range of the stars in the sample. Due to the priority function increasing toward the intermediate age and metallicity isochrone, however, there may be a slight bias toward observing these intermediate age and metallicity stars. This bias is not expected to significantly affect the analysis in this paper, as while the priority function does complicate analysis of the metallicity bias selection, it only effects the uncommon cases where multiple stars were possible candidates for the same slit.

The stellar kinematics in a galaxy encode an important part of a galaxy's history. Stars are probes of the galactic structure as they travel through the galactic potential over time.

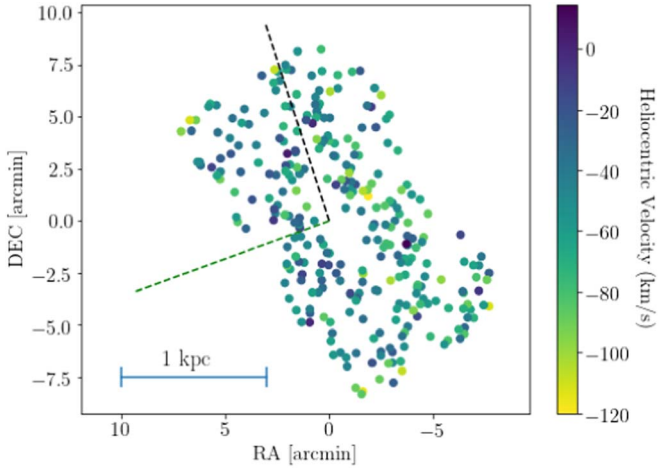

Figure 2. Distribution of stars from Kirby et al. (2013), color coded by heliocentric velocity, with dark blue corresponding to least rapidly approaching and light yellow corresponding to most rapidly approaching. The dotted black line indicates an approximate position angle of the major axis of RGB stars estimated from the RGB isophotes in Figure 8 of Cannon et al. (2012) (18°), while the green line indicates the approximate position angle of the major axis of H I disk from Weldrake et al. (2003) (110°). The velocity gradient apparent from west to east indicates rotation, prolate in the sense of the RGB stars and oblate in the sense of the H I disk. Coordinates are in units of arcmin relative to the center of NGC 6822 (McConnachie 2012). The angular size of 1 kpc is shown in the bottom left for reference; NGC 6822 extends 5 kpc in either direction along the H I major axis and about 1 kpc in either direction along the RGB isophote major axis.

Disruptive events such as mergers or substructure such as tidal streams can be tracked by following stellar groups that are distinct in metallicity and velocity space. Rotation is commonly a criterion referenced to distinguish between dwarf spheroidal and dwarf irregular galaxies with dwarf spheroidals expected to have undergone a significant morphological transition (Mayer et al. 2001).

We examine the kinematics of NGC 6822 through existing measurements of the radial velocities of red giants (Kirby et al. 2014). Because Kirby et al. (2014) restricted their measurements to red giants, our study is sensitive to stellar populations older than ∼1 Gyr. Younger stars, like blue and red supergiants and stars on the upper main sequence, are not present in our sample. Furthermore, the sample is restricted to the central region of the galaxy. Specifically, the measurements are confined to an approximately rectangular region with an area of about $8' \times 15'$. The red giant population extends significantly beyond this region (Cannon et al. 2012).

3. Results

3.1. Prolate Rotation

Figure 2 presents the map of radial velocities of red giants in the center of NGC 6822. Despite the large scatter in stellar velocities, there is a clear velocity gradient across NGC 6822, which shows that the red giant population is rotating. The magnitude of this rotation is about ± 10 km s^{-1}, which is about half of the velocity dispersion of these stars (Kirby et al. 2014). The ratio between the rotation velocity and velocity dispersion indicates the balance of different mechanisms that support the galaxy against gravity. This ratio is about 0.5 for these stars but notably greater than zero.

This nontrivial rotation of the old red giant branch (RGB) stars in Figure 2 is around the major axis of the innermost RGB stars, as estimated from Figure 8 of Cannon et al. (2012). (Battinelli et al. (2006) observed a position angle of about 65° for RGB stars that extend for the entirety of NGC 6822. This angle does not represent the RGB stars in the central core of the galaxy.) Rotation about a major axis is an uncommon phenomenon; most rotation is about a minor axis, such as a spiral galaxy rotating around its minor axis rather than twirling like a flipped coin through space. In fact, prolate rotation is so unusual that it has even been invoked as possible evidence of a merger history for the Andromeda II (Ho et al. 2012) and Phoenix (Kacharov et al. 2017) dwarf galaxies.

If NGC 6822's RGB stars are prolately rotating, this may thus be evidence that NGC 6822 has experienced a merger in its past. This would not be the first time a merger history has been considered for this galaxy; de Blok & Walter (2000) independently proposed a merger history for NGC 6822 due to its morphology and jump in H I disk velocity.

The apparent prolate rotation of the RGB stars is informative even if there was not a merger in NGC 6822's past. If NGC 6822's old population is prolately rotating due to internal processes rather than external mergers, then a dwarf irregular like NGC 6822 could transition into a prolately rotating dwarf spheroidal from just removal of its gas. Wheeler et al. (2017) similarly argued that the low rotation support of the RGB star population in dIrrs could mean that transitioning to dSphs could be done simply by gas removal.

However, the rotation of the RGB stars as seen in Figure 2 is not just around their own major axis, but also along the major axis of the H I disk (Weldrake et al. 2003). Rotation about the same axis as the H I disk makes sense if the RGB stars initially formed from the gas in the disk. However, as the distribution of the central RGB stars does not resemble that of the disk, it is apparent that there is a driver of morphological change between the disk and the central RGB stars. Understanding this transition will help in understanding how dwarf galaxies like NGC 6822 evolve over time.

3.2. Kinematics Evolution

There is clearly a change in the kinematic character between the H I disk and the RGB stars, so the galaxy must have evolved over time. However, how does this transition occur? Was it sudden, such as from a quick merger, or an internal process over a long period of time?

One common diagnostic of the kinematic evolution of a galaxy is an age–velocity dispersion relation (for an example, see Leaman et al. 2017). To approach this problem similarly, we also need to measure the ages and velocity dispersion of our sample of stars.

By classifying stars by age and determining how their kinematics vary as a function thereof, we can probe the transition between the effectively zero-age population of the galaxy (H I gas) and the oldest stellar population of RGBs. One effective method for characterizing ages of stars is to calculate their metallicities: because galaxies increase in metallicity over time, stars with lower metallicity also tend to have been formed earlier. The correlation between age and metallicity can be complicated by stellar migration, as stars forming in separate regions with differing metallicity growth can be mixed by migration, creating metallicity differences in local populations independent of age. While outside the scope of the paper, determination of alpha-to-iron abundances in stars can disambiguate the formation environment of a star from age

evolution, which would reduce uncertainty in this correlation. In the case of NGC 6822, Wyder (2001) found that metallicity is very nearly monotonic with age (Figures 19–22), adding reassurance that metallicity as a proxy for age is a valid assumption.

In addition to age, velocity dispersion information must be considered. Perturbations to a star's orbit are encoded in its velocity dispersion, which gives information about the rotational support of the gas these stars formed from. Alternatively, the star's orbit can be shaped by disruptive events (kinematic collisions or mergers) or a disruptive potential of the host galaxy. To conserve total energy, dispersion of a population also increases if rotation velocity decreases. Given this relation between dispersion and rotation, the ratio of rotational velocity divided by velocity dispersion can be used to understand how the rotational support changes between the gas and stars.

To calculate rotational velocity and velocity dispersion as a function of time, each of the j stars with metallicities within a given range (quintile of [Fe/H]) were grouped together in a bin. Within each of the k bins, velocity dispersion σ within each bin was determined from the line of sight velocities v and uncertainties ϵ from finding the maximum of the likelihood function L_k (as in Wheeler et al. 2017):

$$L_k = \prod_{j=1}^{N} \left(\frac{1}{\sqrt{2\pi(\sigma_k^2 + \epsilon_j^2)}} \times \exp\left[-\frac{1}{2} \frac{(v_j - (\bar{v} + v_{\mathrm{rot},k}\cos(\theta_k - \theta_j)))^2}{\sigma_k^2 + \epsilon_j^2} \right] \right) \quad (1)$$

where $\bar{v}$ is the mean velocity of all stars in the galaxy, θ_k is the angle of the rotation axis for a bin, v_j is the line of sight velocity of star j belonging to bin k, and θ_j is the angle from the center of the galaxy to that star.

From the exponential of Equation (1), the velocity rotation model adopted for a star is the average velocity plus a constant rotation velocity ($v_{\mathrm{rot},k}$) multiplied by an angular projection from the direction of rotation. Wheeler et al. (2017) found that the constant rotation model with just parameter v_{rot} was preferred to their pseudo-isothermal sphere model and is thus used here.

The product in Equation (1) combines all of the fits for each star to maximize simultaneously. The free parameters are the $v_{\mathrm{rot},k}$, σ_k, $\bar{v}$ and θ_k. They were found through maximum likelihood using an MCMC with a Metropolis algorithm and 10^5 links in the chain. A burn-in period of 10^3 links was discarded from the beginning of the chain. This burn-in was found by visual inspection to be sufficient to decouple the chain from the initial choices of free parameters.

With the velocity and metallicity data, plotting the metallicity versus $v_{\mathrm{rot},k}/\sigma_k$ ("rotation support") in each bin results in Figure 3. Notably, there in an increase in the rotation support in NGC 6822 with increasing metallicity, which corresponds to an increased rotation support for younger stars. This behavior is expected if the RGB stars were disrupted from a rotationally dominated disk, or if the rotation support grew over time.

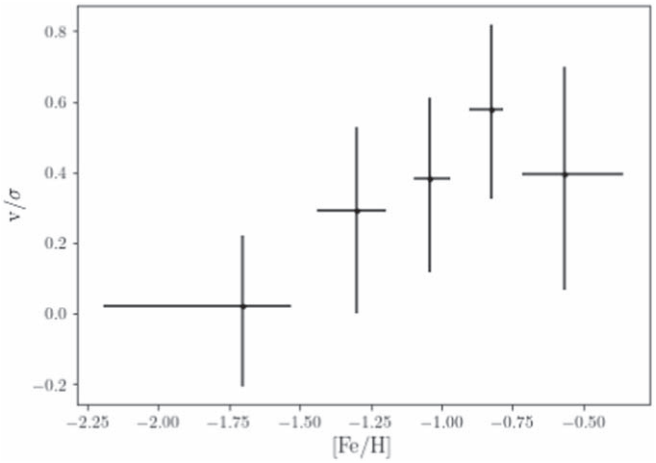

Figure 3. Metallicity vs. rotation support (rotational velocity divided by velocity dispersion) for stars in NGC 6822 separated into five equal-number bins. The errors bars represent 68% confidence intervals. The upward trend in rotation support with metallicity indicates that younger stars are more rotationally supported in NGC 6822. This information is included in the summary of Table 1.

4. Discussion

The evolution of kinematics with metallicity is a tracer of how the galaxy evolved over time, assuming that metallicity increases monotonically with time. However, separating out separate age populations also has a benefit of probing the gravitational potential of a galaxy with separate populations that have their own kinematic properties. Walker & Peñarrubia (2011) effectively utilized this property by extracting out enclosed mass from two independent chemodynamic populations at two separate radii from the Fornax and Sculptor dwarf spheroidal galaxies. Although the two populations trace the same underlying potential, they have separate velocity dispersions and separate physical sizes. Therefore, these two measurements of enclosed mass reveal the slope of the enclosed mass profile. This mass slope can be used to distinguish between cuspy and cored mass profiles, which itself distinguishes between models of galaxy formation (e.g., Navarro et al. 1996, 1997; Mashchenko et al. 2008). Thus, it is clear that the kinematics within multiple-age populations is a powerful probe of galactic evolution.

NGC 6822 has increasing rotation support with increasing metallicity (Figure 3). However, the large uncertainties due in part to the weak rotation and the large velocity dispersion obfuscate any detailed structure in the stellar rotation curve. To understand Figure 3 and the kinematics of NGC 6822 in more detail, we split the rotation support into contributions from rotation and from dispersion in Figure 4. Dispersion notably decreases with increasing metallicity, as noted by Swan et al. (2016). That study separated the galaxy into two populations: metal-rich and metal-poor. Our increased sample size allows us to split the galaxy into five metallicity bins. Our finer view of the evolution of dispersion shows that dispersion steadily decreases across a range of metallicity except for the most metal-rich bin.

The kinetic energy in any metallicity bin is a combination of the energy in rotation and energy in dispersion. We estimated the line of sight rotation velocity v_k using the likelihood function in Equation (1), but the rotation is in the plane of the galaxy, which is inclined relative to the observer. The in-plane

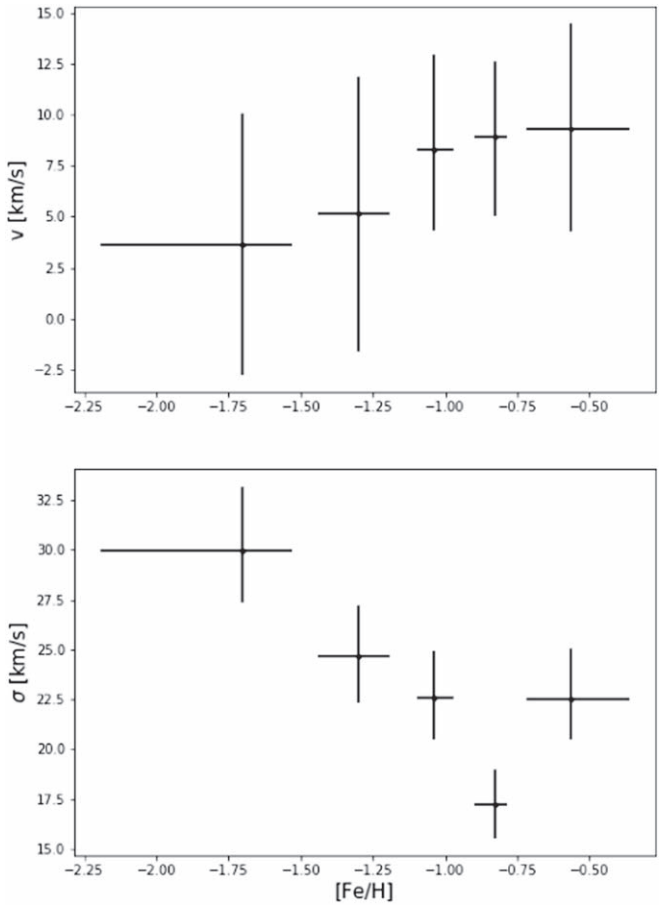

Figure 4. Top: rotation velocity vs. metallicity. Bottom: velocity dispersion vs. metallicity. Taken together, the rotation velocity and velocity dispersion are the components of Figure 3. The velocity dispersion change is more significant than the rotation velocity. The errors bars represent 68% confidence intervals. The upward trend in rotation support with metallicity indicates that more metal-rich, presumably younger stars are more rotationally supported in NGC 6822. This information is included in the summary of Table 1.

rotation velocity is $\frac{v_k}{\sin i}$, and rotational energy per unit mass is $\frac{1}{2}\left(\frac{v_k}{\sin i}\right)^2$. The inclination i of NGC 6822 is 60° (Weldrake et al. 2003). The line of sight dispersion is σ_k also found from the likelihood in Equation (1).

Assuming dispersion is isotropic, kinetic energy per unit mass from the 3D velocity dispersion would be $3 \cdot \frac{1}{2}\sigma_k^2$ in a given bin. However, stellar kinematics are more affected by anisotropy for our centrally concentrated sample of stars compared with the whole stellar population. That is, if dispersion were only radial, line of sight dispersion at the center of the galaxy would encapsulate all energy in dispersion, which would be $\frac{1}{2}\sigma_k^2$. However, a primarily tangential dispersion would indicate that observations of line of sight velocities toward the center of the galaxy vastly underestimate the kinetic energy in the stars. To accommodate this uncertainty, we write kinetic energy in dispersion as $n \cdot \frac{1}{2}\sigma_k^2$, where $n = 1$ corresponds to a purely radial dispersion, $n = 3$ corresponds to isotropic dispersion, and $n > 3$ corresponds to more tangentially dominant dispersion.

For stars distributed over some radius $R_{\rm max}$, this kinetic energy is associated with the gravitational potential energy at the average radius, on the order of $\frac{1}{2}R_{\rm max}$. However, the exact

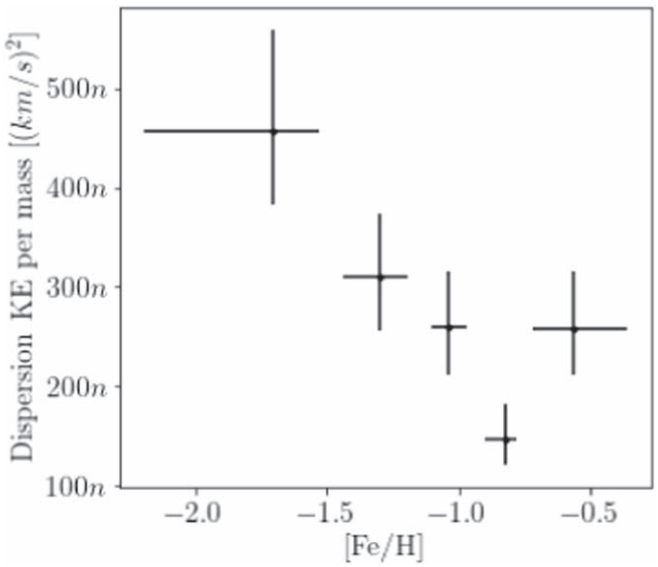

Figure 5. Kinetic energy in dispersion per unit mass of stars in each metallicity bin. The kinetic energy trends in the same way as the dispersion (see Figure 4) because dispersion dominates over rotation. The variable n quantifies uncertainty in anisotropy (see text). Notably, kinetic energy is not constant with metallicity. This information is included in the summary of Table 1.

value of radius depends on the system configuration and anisotropy. More specifically, Wolf et al. (2010) found that enclosed mass at the half-light radius scales as $3G^{-1}\sigma_k^2 r_{1/2}$. There is an enclosed mass dependence on velocity anisotropy, β which is minimized at the 3D (deprojected) half-light radius. In total, kinetic energy at a given metallicity is given by $\frac{1}{2}\left(\frac{v_k}{\sin i}\right)^2 + \frac{n}{2}\sigma_k^2$. The kinetic energy is plotted in Figure 5.

Unsurprisingly, the dispersion component dominates the weak rotation component, so the kinetic energy resembles the dispersion component of Figure 4. Because energy must be conserved but kinetic energy decreases with increasing metallicity, the effective potential energy per unit mass $-\frac{GM_{\rm enclosed}(r)}{r}$ must be increasing with metallicity to balance this effect out. The radius r is measured from the galactic rotation axis, and $M_{\rm enclosed}(r)$ is the total mass enclosed within this radius. The total energy per unit mass is

$$\frac{1}{2}\left(\frac{v_k}{\sin i}\right)^2 + \frac{n}{2}\sigma_k^2 - \frac{GM_{\rm enclosed}(r)}{r} < 0 \qquad (2)$$

and by the virial theorem, twice the kinetic energy of the stars on average should equal the negative of the potential energy:

$$\left(\frac{v_k}{\sin i}\right)^2 + n\sigma_k^2 - \frac{GM_{\rm enclosed}(r)}{r} = 0. \qquad (3)$$

Changes in kinetic energy thus allow measurement of the change in average $-\frac{M_{\rm enclosed}(r)}{r}$ between metallicity bins. Notably, the increase in $-\frac{GM_{\rm enclosed}(r)}{r}$ with metallicity indicates that the average r of each population must decrease with increasing metallicity. That is, metal-rich populations are more centrally concentrated. Such a relation was predicted by Swan et al. (2016) and can be seen in the young versus old stellar population distributions of de Blok & Walter (2006).

Alternatively, the enclosed mass divided by radius can be independently determined from the H I gas velocity curve as a function of radius. A pseudo-isothermal velocity curve model

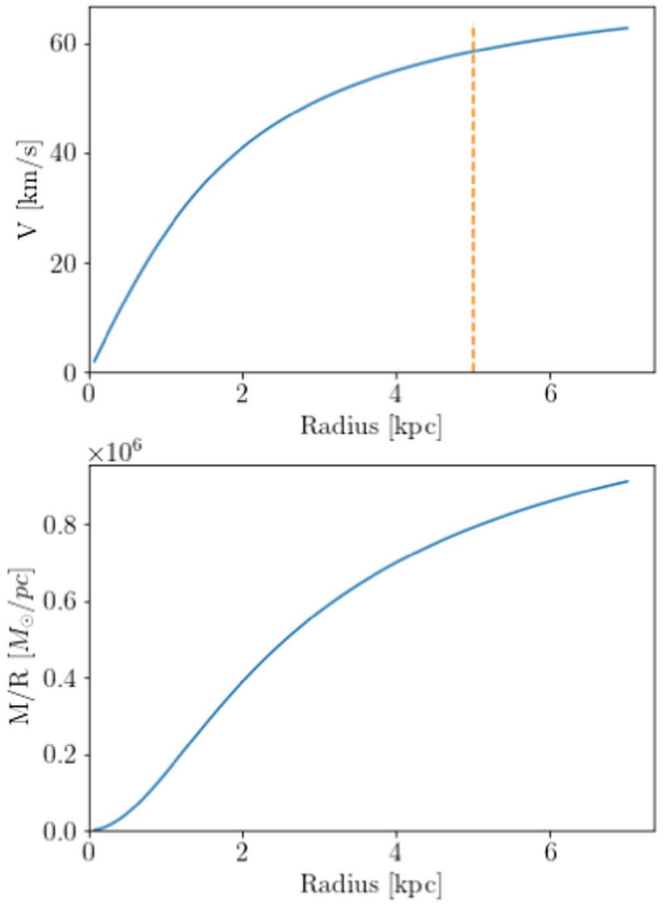

Figure 6. Top: approximate velocity vs. radius from the B24 minimum disk model of Weldrake et al. (2003). The dotted orange line indicates the radial limit of the Weldrake et al. (2003) data, with an extension from the pseudo-isothermal model in velocity beyond this value. Bottom: conversion to enclosed mass divided by radius as a function of radius (i.e., Equation (3) where $\sigma_k = 0$).

used by Weldrake et al. (2003) to model the H I velocity curve is shown in Figure 6. Combined with the enclosed mass versus metallicity relationship (Figure 5), the spatial distribution of the different stellar populations can be probed. The inferred distributions for a purely stellar radial dispersion ($n = 1$) and isotropic dispersion ($n = 3$) are shown in Figures 7 and 8.

As qualitatively predicted earlier, more metal-rich star populations are found toward the center of NGC 6822, and more metal-poor stellar populations have larger effective radii. These observations are consistent with the outside-in star formation processes found in other dwarf galaxies, where star formation became more centrally concentrated over time. Alternatively, negative metallicity gradients have been found to form in dwarf galaxies ($M_* \sim 10^{7\text{-}9.6}\,M_\odot$) by El-Badry et al. (2016, 2018) due to feedback from star formation that drives fluctuations in the galactic potential. These perturbations cause kpc-scale migrations that cause older stellar populations to migrate outward and generate a negative metallicity gradient. Given that NGC 6822 neatly falls within this mass range, and due to its on-off star formation episodes (Wyder 2001; Weisz et al. 2014) that correlate to this model, such an inside-out model may be preferred to explain the more radially extended low-metallicity population in NGC 6822.

The radial distribution of stars with metallicity is about -2 kpc dex^{-1} in the isotropic case and -0.5 kpc dex^{-1} in the radial dispersion case. The lower value is not surprising in the

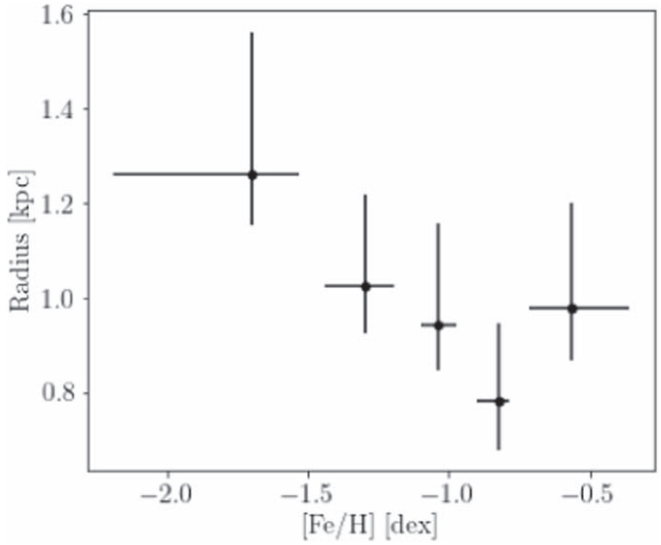

Figure 7. Radius vs. metallicity, combining the enclosed mass vs. metallicity relation (Figure 5) with the velocity data of Weldrake et al. (2003, Figure 6), assuming the stellar dispersion is purely radial. Note that this is not the same as the metallicity gradient (see text). This information is included in the summary of Table 1.

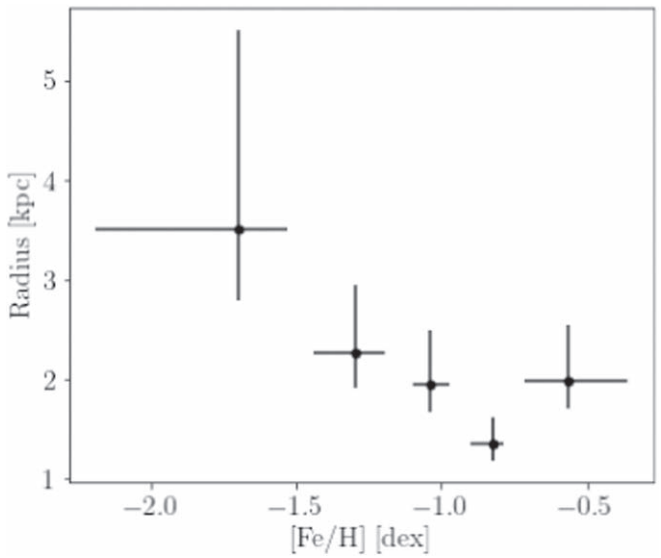

Figure 8. Same as Figure 7, except assuming the stellar dispersion is isotropic. The decreasing velocity curve in H I indicates much further radial distances for metal-poor populations in this case. This information is included in the summary of Table 1.

radial case because radial outflows would more efficiently disperse older stars over time. Furthermore, the distances required in the radial dispersion case are more realistic, being more closely confined the the center of the galaxy than in the isotropic case due to less total energy in the stellar populations. In fact, active star formation histories in the centers of dwarf galaxies have been shown to induce radial anisotropy (El-Badry et al. 2016). These calculated radii indicate a large radial isotropy consistent with an active star formation history. Such a process will be considered more in the next section.

Note that we averaged populations into metallicity bins, and we found the average radii of these bins. In other words, these measurements with units of kpc dex^{-1} indicate how populations at lower metallicities tend to be further away from the center of

Table 1
Summary of the Stellar Binned Data in Figures 3, 4, 5, 7, and 8

[Fe/H] (dex)	Number of Stars	v (km s^{-1})	σ (km s^{-1})	Dispersion K.E. per Mass (km s^{-1})^2	Radius, $n = 1$ (kpc)	Radius, $n = 3$ (kpc)
$-1.70^{+0.17}_{-0.49}$	60	3.6 ± 6.4	$30.0^{+3.2}_{-2.6}$	$449n^{+100\,n}_{-75n}$	$1.3^{+0.3}_{-0.1}$	$3.4^{+1.9}_{-0.7}$
$-1.30^{+0.11}_{-0.14}$	60	5.2 ± 6.7	$24.6^{+2.5}_{-2.3}$	$303n^{+67\,n}_{-54n}$	$1.0^{+0.2}_{-0.1}$	$2.2^{+0.7}_{-0.3}$
$-1.04^{+0.07}_{-0.06}$	58	$8.3^{+4.7}_{-3.9}$	$22.5^{+2.4}_{-2.1}$	$254n^{+57\,n}_{-44n}$	$0.95^{+0.18}_{-0.10}$	$1.9^{+0.5}_{-0.3}$
$-0.82^{+0.04}_{-0.08}$	60	$8.9^{+3.9}_{-3.7}$	$17.2^{+1.8}_{-1.6}$	$148n^{+33\,n}_{-27n}$	$0.75^{+0.15}_{-0.09}$	$1.3^{+0.3}_{-0.2}$
$-0.56^{+0.20}_{-0.15}$	61	$9.3^{+5.0}_{-5.2}$	$22.5^{+2.5}_{-2.1}$	$254n^{+60\,n}_{-45n}$	$0.97^{+0.21}_{-0.11}$	$2.0^{+0.6}_{-0.3}$

the galaxy. This quantity differs from a metallicity gradient (dex kpc^{-1}), which bins together stars at the same radius and then calculates average metallicity at each bin. That is, while the reciprocals of the calculated values indicate there is a negative metallicity gradient, which is considered in the rest of the analysis of this paper, they cannot be directly compared with metallicity gradients in NGC 6822 (e.g., Swan et al. 2016, who found that metallicity dispersion prevented a precise analysis). Data summarizing the results from this paper across each metallicity bin are presented for convenience in Table 1.

4.1. Formation History

We can also consider why the metal-rich, young stars are more centrally concentrated. Unlike in spiral galaxies where star formation occurs in the arms rather than the center, the younger star distribution in NGC 6822 is centrally concentrated. However, many dSphs have been found to have centrally concentrated younger stellar populations.

One possibility for a negative metallicity gradient is that stars in NGC 6822 formed in a disk, but star formation in outer regions of the galaxy decreased more rapidly with time, due to reasons such as ionization of the outer H I disk (Kawata et al. 2006) or merely gas depletion. This can explain why dSphs stop forming stars in their outskirts first, yet the dwarf irregular NGC 6822 still has plenty of gas. This does not explain why the the youngest, most metal-rich stars are at a slightly larger radius than the second most metal-rich bin.

Another possibility is that a merger event occurred, funneling new gas toward the center of the galaxy while also relocating old stellar populations to larger radii. NGC 6822 has been speculated to have a merger event in its history, invoked by de Blok & Walter (2000) to explain NGC 6822s H I velocity curve. Such an event may be expected to bifurcate the stellar population, with separable old and young populations, whereas the observed metallicity gradient in NGC 6822 seems to be more continuous between bins. However, it may be possible for smaller mergers over time to smooth out such a gradient (Benítez-Llambay et al. 2016).

One possible explanation for the distribution of the RGB stars appearing to rotate in a prolate sense is that these stars trace a dynamical bar along the line of sight. If such a bar existed, it would affect the dynamics of the rest of the galaxy, perhaps in a noticeable way. In a set of simulations by Friedli et al. (1994), abundance gradients in barred galaxies were found to be flattened with a possibly metal-rich center. This prediction does not match with the the observed metallicity gradient for NGC 6822 (e.g., Figure 8), indicating that the RGB population may not occupy a bar. However other studies, such as Pérez et al. (2009), Zhuang et al. (2019), found a more complicated family of possibilities, with positive, zero, and negative metallicity gradients in barred galaxies. The negative metallicity gradients (corresponding to NGC 6822's case) were explained as originating from the disk not having enough time to flatten out. Such negative metallicity gradients also tend to correlate with positive age gradients (younger populations toward the center). This metallicity gradient relation is intriguing, but it does not appear to distinguish between other possible formation scenarios.

Radial migration of stars has also been used to explain metallicity gradients in galaxies: unordered radial migration may dilute an initially strong metallicity gradient. Radial migration can be induced by mergers, perturbations by companion galaxies, or galactic substructures. Loebman et al. (2016) were able to explain the varied metallicity distributions in the Milky Way as a function of radius by following radial migration in simulations. High-metallicity stars formed toward the center of the galaxy but migrated outward, enriching and skewing the outer radial metallicity distributions. In dwarf galaxies, an independent and dominant driver of radial migration may be induced by feedback during bursty star formation histories. El-Badry et al. (2016) found that in $M_* = 10^{7-9.6}\,M\odot$ dwarf galaxies, feedback disrupting star formation in the center of the galaxy systematically drove out stars toward the galactic edges, creating metallicity gradients similar to that observed in our data for NGC 6822. Notably, such a high central star formation history would induce large, preferentially radial inflows and outflows of stars and gas during star formation bursts, which would also be consistent with the kinematic results of the previous section.

5. Summary

In conclusion, NGC 6822 is a promising candidate to study dwarf irregular populations and dynamics due to its mass and proximity. RGB archival data from Kirby et al. (2013) revealed a 10 km s^{-1} rotation in the center of the galaxy, approximately half that of the dispersion. This rotation is unusual in that it is prolate relative to the distribution of RGB stars, though it also matches the rotation of the H I disk. Due to the large number of stars and precise metallicity of the data, the rotation and velocity dispersion of the RGB population were measured in five metallicity bins. The kinematics across the bins were compared with the gas, which probes the same potential as the stars, to determine the radial extent of each population. A radial gradient of -0.5 kpc dex^{-1} (in the radial case) was found by relating the observed stellar kinematics to position via NGC 6822's H I velocity curve. Negative metallicity gradients are sometimes correlated with outside-in star formation in a galaxy. However, NGC 6822's multiple episodes of star formation may instead indicate that stellar feedback induced migration of preferentially older stars out of the center of the galaxy.

The authors thank the anonymous referee for the input which improved this paper.

This material is based upon work supported by the National Science Foundation under grant Nos. AST-1636426 and AST-1847909. E.N.K. gratefully acknowledges support from a Cottrell

Scholar award administered by the Research Corporation for Science Advancement, as well as funding from generous donors to the California Institute of Technology. M.B.K. acknowledges support from NSF CAREER award AST-1752913, NSF grant AST-1910346, NASA grant NNX17AG29G, and HST-AR-15006, HST-AR-15809, HST-GO-15658, HST-GO-15901, and HST-GO-15902 from the Space Telescope Science Institute, which is operated by AURA, Inc., under NASA contract NAS5-26555. Support for C.W. was provided by NASA through the NASA Hubble Fellowship grant HST-HF2-51449.001-A, awarded by the Space Telescope Science Institute, which is operated by the Association of Universities for Research in Astronomy, Inc., for NASA, under contract NAS5-26555.

We are grateful to the many people who have worked to make the Keck Telescope and its instruments a reality and to operate and maintain the Keck Observatory. The authors extend special thanks to those of Hawaiian ancestry on whose sacred mountain we are privileged to be guests. Without their generous hospitality, none of the observations presented herein would have been possible.

Facility: Keck:II (DEIMOS).

ORCID iDs

Brent Belland https://orcid.org/0000-0003-1950-448X
Evan Kirby https://orcid.org/0000-0001-6196-5162
Michael Boylan-Kolchin https://orcid.org/0000-0002-9604-343X

References

Battinelli, P., Demers, S., & Kunkel, W. E. 2006, A&A, 451, 99
Benítez-Llambay, A., Navarro, J. F., Abadi, M. G., et al. 2016, MNRAS, 456, 1185
Cannon, J. M., O'Leary, E. M., Weisz, D. R., et al. 2012, ApJ, 747, 122
de Blok, W. J. G., & Walter, F. 2000, ApJL, 537, L95
de Blok, W. J. G., & Walter, F. 2006, AJ, 131, 343
de Vaucouleurs, G., de Vaucouleurs, A., & Corwin, H. G. 1976, Second Reference Catalogue of Bright Galaxies Containing Information on 4364 Galaxies with Reference to Papers Published Between 1964 and 1975 (Austin, TX: Univ. Texas Press)
El-Badry, K., Quataert, E., Wetzel, A., et al. 2018, MNRAS, 473, 1930
El-Badry, K., Wetzel, A., Geha, M., et al. 2016, ApJ, 820, 131
Faber, S. M., Phillips, A. C., Kibrick, R. I., et al. 2003, Proc. SPIE, 4841, 1657
Feast, M. W., Whitelock, P. A., Menzies, J. W., & Matsunaga, N. 2012, MNRAS, 421, 2998
Friedli, D., Benz, W., & Kennicutt, R. 1994, ApJL, 430, L105
Gallart, C., Aparicio, A., Bertelli, G., & Chiosi, C. 1996, AJ, 112, 2596
Ho, N., Geha, M., Munoz, R. R., et al. 2012, ApJ, 758, 124
Hopkins, P. F., Kereš, D., Oñorbe, J., et al. 2014, MNRAS, 445, 581
Hubble, E. P. 1926, ApJ, 64, 321
Iorio, G., Fraternali, F., Nipoti, C., et al. 2017, MNRAS, 466, 4159
Kacharov, N., Battaglia, G., Rejkuba, M., et al. 2017, MNRAS, 466, 2006
Kaufmann, T., Wheeler, C., & Bullock, J. S. 2007, MNRAS, 382, 1187
Kawata, D., Arimoto, N., Cen, R., & Gibson, B. K. 2006, ApJ, 641, 785
Kirby, E. N., Bullock, J. S., Boylan-Kolchin, M., Kaplinghat, M., & Cohen, J. G. 2014, MNRAS, 439, 1015
Kirby, E. N., Cohen, J. G., Guhathakurta, P., et al. 2013, ApJ, 779, 102
Komiyama, Y., Okamura, S., Yagi, M., et al. 2003, ApJL, 590, L17
Leaman, R., Mendel, J. T., Wisnioski, E., et al. 2017, MNRAS, 472, 1879
Letarte, B., Demers, S., Battinelli, P., & Kunkel, W. E. 2002, AJ, 123, 832
Loebman, S. R., Debattista, V. P., Nidever, D. L., et al. 2016, ApJL, 818, L6
Mashchenko, S., Wadsley, J., & Couchman, H. M. P. 2008, Sci, 319, 174
Massey, P., Olsen, K. A. G., Hodge, P. W., et al. 2007, AJ, 133, 2393
Mayer, L., Governato, F., Colpi, M., et al. 2001, ApJ, 559, 754
McConnachie, A. W. 2012, AJ, 144, 4
Navarro, J. F., Frenk, C. S., & White, S. D. M. 1996, ApJ, 462, 563
Navarro, J. F., Frenk, C. S., & White, S. D. M. 1997, ApJ, 490, 493
Pérez, I., Sánchez-Blázquez, P., & Zurita, A. 2009, A&A, 495, 775
Postman, M., & Geller, M. J. 1984, ApJ, 281, 95
Sandage, A. 2005, ARA&A, 43, 581
Spekkens, K., Urbancic, N., Mason, B. S., Willman, B., & Aguirre, J. E. 2014, ApJL, 795, L5
Swan, J., Cole, A. A., Tolstoy, E., & Irwin, M. J. 2016, MNRAS, 456, 4315
Thompson, G. P., Ryan, S. G., & Sibbons, L. F. 2016, MNRAS, 462, 3376
Valenzuela, O., Rhee, G., Klypin, A., et al. 2007, ApJ, 657, 773
Walker, M. G., & Peñarrubia, J. 2011, ApJ, 742, 20
Weisz, D. R., Dolphin, A. E., Skillman, E. D., et al. 2014, ApJ, 789, 147
Weldrake, D. T. F., de Blok, W. J. G., & Walter, F. 2003, MNRAS, 340, 12
Wheeler, C., Pace, A. B., Bullock, J. S., et al. 2017, MNRAS, 465, 2420
Wolf, J., Martinez, G. D., Bullock, J. S., et al. 2010, MNRAS, 406, 1220
Wyder, T. K. 2001, AJ, 122, 2490
Zhuang, Y., Leaman, R., van de Ven, G., et al. 2019, MNRAS, 483, 1862